Laser-Induced Spectral Diffusion of T Centers in Silicon Nanophotonic Devices

Xueyue Zhang,[1,2,*] Niccolò Fiaschi,[1,2,3] Lukasz Komza,[2,4] Hanbin Song,[4,5] Thomas Schenkel,[3] and Alp Sipahigil[1,2,4,†]

[1] *Department of Electrical Engineering and Computer Sciences, University of California, Berkeley, Berkeley, California 94720, USA*

[2] *Department of Physics, University of California, Berkeley, Berkeley, California 94720, USA*

[3] *Accelerator Technology & Applied Physics Division, Lawrence Berkeley National Laboratory, Berkeley, California, 94720, USA*

[4] *Materials Sciences Division, Lawrence Berkeley National Laboratory, Berkeley, California 94720, USA*

[5] *Department of Materials Science and Engineering, University of California, Berkeley, Berkeley, California 94720, USA*

(Received 18 April 2025; revised 13 July 2025; accepted 12 August 2025; published 16 September 2025)

Color centers in silicon are emerging as spin-photon interfaces operating at telecommunication wavelengths. The nanophotonic device integration of silicon color centers via ion implantation leads to significant optical-linewidth broadening, which makes indistinguishable photon generation challenging. Here, we study the optical spectral diffusion of T centers in a silicon photonic crystal cavity. We investigate the linewidth-broadening timescales and origins by measuring the temporal correlations of the resonance frequency under different conditions. Spectral hole-burning measurements reveal no spectral broadening at short timescales from 102 ns to 725 ns. We probe broadening at longer timescales using a check pulse to herald the T-center frequency and a probe pulse to measure the frequency after a wait time. The optical resonance frequency is stable up to 3 ms in the dark. Laser pulses below the silicon band gap applied during the wait time lead to linewidth broadening. Our observations establish laser-induced processes as the dominant spectral-diffusion mechanism for T centers in devices and inform materials and feedback strategies for indistinguishable photon generation.

DOI: 10.1103/x2cv-2gcw

I. INTRODUCTION

Color centers in silicon have emerged as a promising platform for quantum information science [1–3] due to their compatibility with scalable photonic integration and manufacturing [4]. Among the silicon color centers, T centers have shown highly coherent ground-state electron and nuclear spins [5]. With an optical transition in the telecommunication O band, the T center has become a spin-photon interface candidate suitable for quantum networking and communication applications [3,6].

A major challenge for indistinguishable photon generation with color centers is optical-linewidth broadening. The linewidth broadening includes homogeneous broadening involving processes faster than the emitter lifetime and slow spectral diffusion usually due to electric field noise [7,8]. For color centers in diamond [9,10] and silicon carbide [11–13], their integration into nanophotonic devices exacerbates the spectral diffusion [14–18] and the laser excitation plays a significant role in introducing the spectral diffusion via reconfiguration of the local charge environment or ionization of the color centers [17–19]. For silicon T centers, photoluminescence-excitation (PLE) linewidths as narrow as 33 MHz have been observed in ultra-high-quality bulk silicon at 1.4 K [5]. However, in photonic devices and at higher temperatures, both homogeneous broadening and spectral diffusion contribute to further linewidth broadening. For example, in typical nanophotonic devices at 4 K, the spectral diffusion (a few gigahertz) is about an order of magnitude larger than the homogeneous broadening (hundreds of megahertz) and 4 orders of magnitude larger than the lifetime-limited linewidth (a few hundred kilohertz), creating a large

*Present address: Department of Applied Physics and Applied Mathematics, Columbia University, New York, New York 10027, USA.

†Contact author: alp@berkeley.edu

Published by the American Physical Society under the terms of the Creative Commons Attribution 4.0 International license. Further distribution of this work must maintain attribution to the author(s) and the published article's title, journal citation, and DOI.

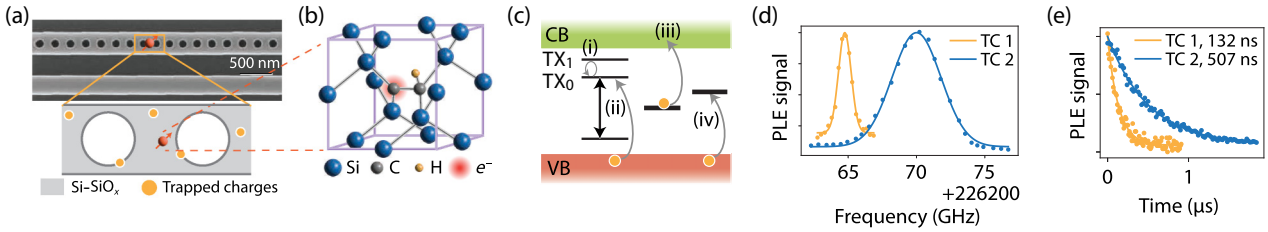


FIG. 1. The optical-linewidth broadening of T centers. (a) A scanning-electron-microscopy (SEM) image of the device, a photonic crystal cavity coupled to a waveguide. The enlarged schematics illustrate a T center with nearby fluctuating charge traps in the bulk and on the surfaces. (b) The atomic structure of a T center. (c) The T-center level structure and possible mechanisms leading to linewidth broadening: (i) the thermal transition between TX_0 and TX_1 states; (ii) ionization; (iii),(iv) the charge transfer between a trap state and (iii) the conduction band (CB) or (iv) the valence band (VB). (d),(e) The (d) photoluminescence-excitation (PLE) spectra and (e) cavity-enhanced lifetimes of two T centers under study.

gap between the lifetime-limited linewidth and the measured spectral linewidth [3]. Although the homogeneous linewidths of T centers in nanophotonic devices are comparable to the results in bulk silicon [20], the causes and timescales of the total linewidth broadening for T centers have not been explored.

Here, we study the homogeneous linewidth and spectral diffusion of T centers in a photonic crystal cavity. We use spectral hole burning and the tunable T-center lifetime via the Purcell effect to investigate the linewidth-broadening effects within the T-center lifetime. The homogeneous linewidth is unchanged when the lifetime is tuned from 102 ns to 725 ns. To study linewidth broadening at longer timescales, we use check-probe spectroscopy [19] and find that the optical resonance is stable without broadening in the dark up to 3 ms. We identify the cause of linewidth broadening as laser excitation by inserting laser pulses in the check-probe sequence. We show that this laser-induced spectral diffusion is not a resonant effect associated with T-center excitation.

II. DEVICE AND T-CENTER PLE MEASUREMENTS

We study the spectral properties of T centers in a one-dimensional photonic crystal cavity, as shown in Fig. 1(a). The thickness of the silicon device layer is 220 nm and the minimal width of silicon between adjacent holes at the electric field maximum is 172 nm. Further details of the device, fabrication, and T-center creation are discussed in Ref. [21].

The spectral properties of T centers [atomic structure shown in Fig. 1(b)] are influenced by the structure of the excited states that form a bound-exciton series. The first two excited states, TX_0 and TX_1, are split by a small energy gap of around 1.76 meV [5] [Fig. 1(c)]. This small gap enables rapid thermal transitions between TX_0 and TX_1 and introduces a broadening that is strongly dependent on the local temperature [Fig. 1(c), process (i)]. The T-center thermal broadening is a rapid process compared to the lifetime of a T center [5], even with Purcell enhancement [21–23], thus contributing to the homogeneous linewidth. Local charge-trap reconfiguration and an ionization-induced local charge shift are other common sources for spectral diffusion in color centers [19,24–29]. For T centers, the ionization [process (ii) in Fig. 1(c)] and charge-trap reconfiguration [processes (iii) and (iv) in Fig. 1(c)] happen at longer timescales than thermal broadening, resulting in further broadening of the linewidth. We denote the instantaneous frequency of the ground-to-TX_0 optical transition as $\omega_T(t)$. We investigate the frequency fluctuation distribution $(\omega_T(t+\tau) - \omega_T(t))$ at the timescale of τ and the corresponding linewidth $\gamma(\tau)$. Specifically, the spectral diffusion can be modeled as a spectral random walk and is known to exhibit a linearly increasing linewidth at short times $\gamma(\tau) = \gamma_d \tau$ [19,30]. We study the diffusion rate γ_d under different conditions in our system.

We study T centers in a single cavity where T center 1 (TC1) is measured in the first cooldown and T center 2 (TC2) in the second cooldown after a room-temperature thermal cycling. During the first (second) cooldown, only TC1 (TC2) appears within the cavity resonance at 226.27 THz. We measure the PLE spectrum at an optical power below the power-broadening limit. The FWHM linewidths obtained from Gaussian fits are 1.10 GHz and 4.22 GHz, respectively, for TC1 and TC2 [Fig. 1(d)]. With a single-trace averaging time of 1.7 h, this linewidth represents the long-time linewidth $\gamma(\tau \to \infty)$. We have not observed spectral wandering between traces for single-trace averaging time ranges from minutes to hours. The Purcell-enhanced optical lifetimes T_1 of TC1 and TC2 are extracted to be 132 ns and 507 ns, respectively [Fig. 1(e)].

III. PROBING HOMOGENEOUS LINEWIDTH USING SPECTRAL HOLE BURNING

The linewidth broadening within the optical lifetime, i.e., the homogeneous linewidth, can be measured via

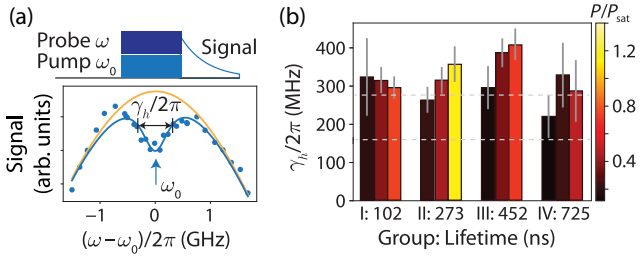


FIG. 2. Spectral hole burning. (a) The pulse sequence (upper panel) and a typical hole-burning spectrum (lower panel) by sweeping the probe-laser frequency. (b) The spectral hole width of four lifetime groups, with the bar color indicating the total measurement power. The upper dashed line shows the average hole width of the lowest-power measurement across the four groups, while the lower dashed line shows the thermal-limited hole width calculated from the cryostat base temperature.

spectral hole burning [20,31]. We send a pump pulse to TC1 at its center frequency $\omega_0 = \omega_T$ and sweep the frequency of a probe pulse ω across the T-center spectral range. The two pulses are sent in simultaneously and the length is set to 1 μs to reach the steady state before we collect the emission from the T center as the signal [Fig. 2(a) top]. We note that because of the saturation spectroscopy nature of the hole-burning measurement, the timescale of the linewidth broadening is set by the lifetime of the emitter instead of the pulse length [31]. Due to the saturation of the single-photon emitter, the pump laser excites the emitter when it is close to the pump frequency and suppresses the subsequent excitation from the probe laser. The saturation effect is absent when the emitter drifts away from the pump-laser frequency. Therefore, this sequence creates a spectral hole for the single emitter [Fig. 2(a) bottom]. The width of the spectral hole γ_h is twice the homogeneous optical linewidth of the emitter $\gamma(\tau = T_1)$ at low pump and probe power [31].

To investigate the linewidth change for $\tau < 1\,\mu$s, we control the optical lifetime of TC1 by changing the cavity-TC1 detuning via gas tuning of the cavity frequency [21]. At each lifetime (102, 273, 452, 725) ns, we extract γ_h from the Lorentzian fit of the hole on a Gaussian background. To ensure that the hole width is in the low-power regime, we measure three different total waveguide powers during the pump and probe pulses for each lifetime [Fig. 2(b)]. There is no clear trend across different lifetime groups, suggesting that no additional homogeneous broadening from laser-related processes occurs in 102 ns $< \tau <$ 725 ns, even under laser power close to saturation power P_{sat}.

The average $\gamma_h/2\pi$ for the four groups at the lowest waveguide power is 277 MHz, which is larger than the hole width of 161 MHz calculated from base temperature $T = 3.41$ K and TX_0-TX_1 splitting of 1.76 meV [5]. The difference indicates the higher local temperature at the sample (Appendix A) or smaller TX_0-TX_1 splitting.

IV. PROBING SPECTRAL DIFFUSION USING CHECK-PROBE SPECTROSCOPY

We investigate the timescale of the spectral diffusion, where the optical linewidth further broadens from its homogeneous linewidth by processes slower than the optical lifetime. In this study, we employ the check-probe spectroscopy [19] on TC2. We send a check pulse at frequency ω_0, wait for time τ, and send another probe-laser pulse at frequency ω. We collect the counts from the T center in both the emission window after the check pulse and the one after the probe pulse. A click in the check emission window indicates that the T center is close to resonance with ω_0 up to the power-broadened instantaneous linewidth. After wait time τ, the T-center frequency distribution with possible spectral diffusion in this timescale can be probed by sweeping the probe-laser frequency ω. An example at $\tau = 2.5$ μs is shown in Fig. 3(a). The *unconditional* line shape is measured by all signal counts per pulse in the probe emission window at different ω. The *conditional* line shape is obtained by counting the clicks

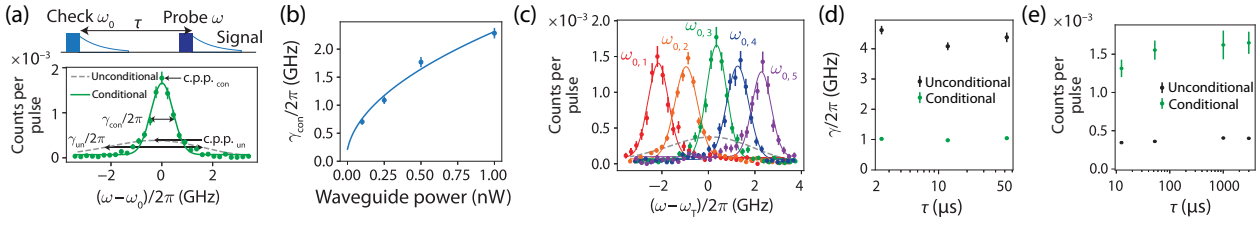


FIG. 3. Check-probe spectroscopy. (a) The pulse sequence (upper panel) and typical unconditional and conditional spectra (lower panel) from the check-probe spectroscopy. (b) The conditional linewidth as a function of the laser pulse power in the waveguide, where the check and probe pulses are set at the same power. (c) The conditional line shape at check detunings $((\omega_{0,j} - \omega_T)/2\pi)$ of $(-2.15, -0.96, 0.35, 1.26, 2.28)$ GHz for j from 1 to 5. The dashed curve shows the unconditional spectrum. (d) The unconditional and conditional linewidths for $\tau = 2.5, 12.5$, and 52.5 μs. (e) The unconditional and conditional peak counts per pulse for $\tau = 12.5, 52.5, 1000, 3000\,\mu$s.

in the emission window only when there is a click in the check emission window before this probe. The conditional linewidth $\gamma_{\mathrm{con}}/2\pi = 1.02\,\mathrm{GHz}$ is narrower than the unconditional PLE linewidth $\gamma_{\mathrm{un}}/2\pi = 4.62\,\mathrm{GHz}$. Additionally, the counts per pulse (CPP) click rate in the probe window are higher in the case of the conditional line shape because of the narrower spectral linewidth. The observations suggest that once the T-center frequency is confirmed in the check window, the spectral diffusion in the waiting time is less severe compared to the PLE results.

Before studying check-probe spectroscopy under various conditions, we first explore the broadening effects associated with the laser power in the measured conditional linewidth [Fig. 3(b)] with $\tau = 2.5\,\mu\mathrm{s}$. These broadening effects include both power broadening and possible laser-induced linewidth broadening. The check and probe pulses are tuned to be at the same power. Using the power-broadening relation $\gamma_{\mathrm{con}} = \gamma_{\mathrm{con},0}\sqrt{1 + P/P_{\mathrm{sat}}}$, where P_{sat} is the saturation power and $\gamma_{\mathrm{con},0}$ is the zero-power conditional linewidth, we obtain $\gamma_{\mathrm{con},0}$ to be $0.2 \pm 0.4\,\mathrm{GHz}$. Although obtaining an accurate zero-power linewidth will require more measurements in the low-power regime with a low count rate, the conditional analysis already reveals the power dependence previously not observable due to the large spectral linewidth of PLE. The power-dependence measurement also indicates that the limit of γ_{con} is mainly set by laser-power-related broadening instead of spectral diffusion within the wait window of $\tau = 2.5\,\mu\mathrm{s}$. In the following measurements, we use the waveguide power of 0.25 nW to reduce the power-broadening effect while maintaining a reasonable count rate.

To confirm that the T-center spectral diffusion is around the pinned frequency by the check pulse, we have repeated the measurements at different values of ω_0 around the PLE T-center frequency distribution. The absolute count rate in the check window drops as ω_0 is detuned away from ω_T, requiring a longer acquisition time. The linewidth and click rate per pulse in the conditional line shape remain unchanged, with the conditional center frequency set by ω_0 [Fig. 3(c)].

Further, we investigate whether the spectral diffusion shows up at long wait time τ. For τ up to $52.5\,\mu\mathrm{s}$, we sweep the probe frequency ω and extract the linewidth [Fig. 3(d)], showing that the conditional linewidth does not increase with the wait time in this regime. For longer wait times τ up to 3 ms, we use the CPP click rate at $\omega = \omega_0$ [Fig. 3(e)] as a measure of how likely the T-center frequency is to remain stable without drifting away, where the drift will cause a decrease in the CPP. The value of $\mathrm{CPP}_{\mathrm{con}}$ shows a slight increase within the error bar for long wait times, suggesting no observable increase in conditional linewidth. In summary, up to $\tau = 3\,\mathrm{ms}$, we do not observe spectral diffusion induced by the dark wait time.

V. LASER-INDUCED SPECTRAL DIFFUSION

To investigate the cause of spectral diffusion, we modify the check-probe sequence and insert a perturbation sequence in the middle. The perturbation sequence consists of repeated laser pulses [Fig. 4(a)], which have been observed to induce spectral diffusion in diamond and SiC [17,19]. First, we set the perturbation-laser frequency to be resonant with the center frequency of TC2 ω_T, with an individual pulse duration of 200 ns and a period of $2.5\,\mu\mathrm{s}$. The check pulse is resonant ($\omega_0 = \omega_T$) and we sweep the frequency of the probe pulse to extract the conditional linewidth when clicks happen in both the check and probe windows. For perturbation-pulse number N ranging from 0 (no perturbation pulse) to 9, the linewidth increases from 1.16 GHz to 2.98 GHz [Fig. 4(b)], approaching the PLE linewidth. The corresponding line shapes [Fig. 4(c)] change gradually from peaked to flattened with increasing N. At laser-pulse number $N \leq 4$, the conditional linewidth $\gamma/2\pi$ increases linearly with the laser pulse at a rate of 1.45 GHz per microsecond of laser pulse (Appendix C). The fluctuation of the linewidth at large N results from the photon shot noise as the line shape flattens and the center frequencies accumulate fewer counts than small N results. Additionally, we observe an increase of the linewidth with increased perturbation-pulse power when maintaining the duration and number of the perturbation pulses (Appendix B).

This laser-induced spectral diffusion could be due to the local charge-environment change from either resonant effects such as the ionization of TC2 itself [(ii) in Fig. 1(c)] or the reconfiguration of nearby charge traps [(iii) and (iv) in Fig. 1(c)]. To distinguish these two effects,

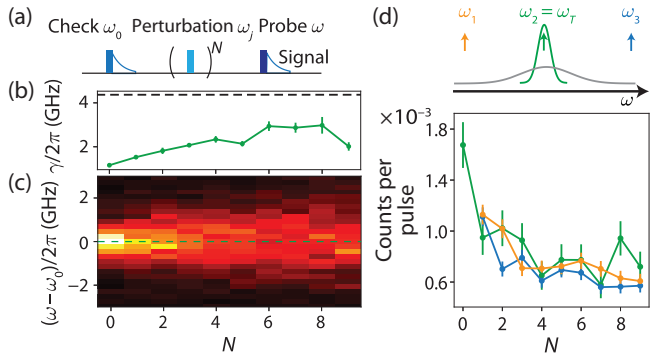


FIG. 4. Laser-induced spectral diffusion. (a) The pulse sequence with N laser perturbation pulses inserted between the check pulse and probe pulse. (b),(c) The (b) linewidth and (c) line shape of the conditional spectra for N perturbation pulses. (d) Top: schematics of the three perturbation-laser frequency relative to the T-center frequency and linewidth, with the green curve showing the conditional line shape and the gray curve showing the unconditional line shape. Bottom: the peak counts per pulse versus N for the three perturbation-laser frequency, with the color corresponding to the arrow color in the top panel.

we repeat the measurements with off-resonant perturbation pulses. We choose the perturbation-pulse frequency to be either −5.1 GHz or 5.95 GHz detuned from TC2 center frequency ω_T. These detunings are large enough to avoid the excitation of TC2 [illustrated in Fig. 4(d)], especially after its frequency is heralded by the check pulse. On the other hand, these detunings are small compared to the cavity linewidth of 17.9 GHz, enabling effective coupling of photons into the cavity. Similar to the previous section, we use the peak CPP, which is inversely proportional to the linewidth, as a measure of the height of the line shape. The resonant CPP extracted directly from Fig. 4(c) is used as a reference. The perturbations with different detunings follow the same trend as the resonant perturbation [Fig. 4(d)], indicating that the resonant effects, including the T-center ionization, are not the major source for laser-induced spectral diffusion for T centers.

VI. CONCLUSIONS AND DISCUSSION

Our spectral hole-burning and check-probe spectroscopy results reveal the possible origins and the relevant timescales of T-center linewidth broadening in nanophotonic devices. The observations suggest that at short timescales below hundreds of nanoseconds, the homogeneous linewidth does not increase with the optical lifetime in the current experiments. Without a laser perturbation, the T center in the dark can preserve its frequency for at least 3 ms. Laser perturbation, even with frequencies below the silicon band gap, plays a major role in introducing spectral broadening. The broadband nature of the effect suggests that broadening is due to the reconfiguration of the nearby charge environment instead of the ionization of the T center itself.

These conclusions can be used to design more efficient pulse sequences for indistinguishable photon generation with T centers. As an example, the entanglement generation between two T centers using emitted photon interference [18,32–36] requires frequency matching of these two emitters. Instead of waiting for the two emitters to arrive at the same frequency among the frequency jitters, each emitter can be prepared independently using the check pulse, with a click heralding successful preparation at the laser frequency [34,35,37]. The emitter prepared first can preserve its frequency in the dark while waiting for the other emitter to be ready. This heralded preparation method avoids repeating the full sequence numerous times. Instead, the repeat-until-success part only happens for the short emitter excitation sequence. On the other hand, the spectral diffusion dominated by laser-induced charge reconfiguration may pose a challenge with regard to preserving the emitter frequency during spin initialization using optical pumping. Detailed studies considering the specific power and duration of the optical-pumping pulse will be necessary to determine whether the optical transition frequency can be prepared before the spin initialization.

This study also raises questions for further exploration. Carrying out the check-probe spectroscopy in a waveguide [20,38] instead of the photonic crystal cavity could provide broader-band information about the charge-trap response in silicon. Further study is needed to investigate the origin and dominant location of the charge traps, which can be broadly categorized as bulk charge traps and surface charge traps. Some surface charge traps at the Si-SiO_2 interfaces such as the P_b centers are well studied [39–41]. The use of surface-passivation techniques [42] or changing the nanophotonic structure dimension will help to separate the contribution of different sources, which could lead to solutions to reduce the spectral diffusion. The current check-probe spectroscopy linewidth is limited by laser-power-related broadening. The use of Hong-Ou-Mandel interference [43–46] enables access to the power-broadening-free linewidth at various wait times. Lastly, cooling the device to 1 K will exponentially lower the thermal-limited linewidth [5,20]. The lower temperature could unveil frequency-jitter mechanisms currently masked by the thermal linewidth.

Note added. We have recently become aware of the related work by Bowness and Meynell *et al*. [47].

ACKNOWLEDGMENTS

We thank Zi-Huai Zhang and Mi Lei for helpful discussions and feedback on the manuscript. This work was primarily supported by the U.S. Department of Energy, Office of Advanced Scientific Computing Research (ASCR), Office of Science, under Contract No. DE-AC02-05CH11231 and Berkeley Lab FWP FP00013429. L.K. and A.S. acknowledge support from the National Science Foundation (NSF) (QLCI program through Grant No. OMA-2016245, and Award No. 2137645). X.Z. acknowledges support from the Miller Institute for Basic Research in Science. The devices used in this work were fabricated at the Berkeley Marvell NanoLab.

DATA AVAILABILITY

The data that support the findings of this paper are openly available [48].

APPENDIX A: SPECTRAL HOLE BURNING: SETUP AND TEMPERATURE DEPENDENCE

We use the setup depicted in Fig. 5 for the spectral hole burning. Two lasers (Santec TLS-570 and Instatune FP4209) are locked using a wave meter (High Finesse WS/6-200) with a proportional integral differential (PID) loop. After getting combined at the 50 : 50 beam splitter

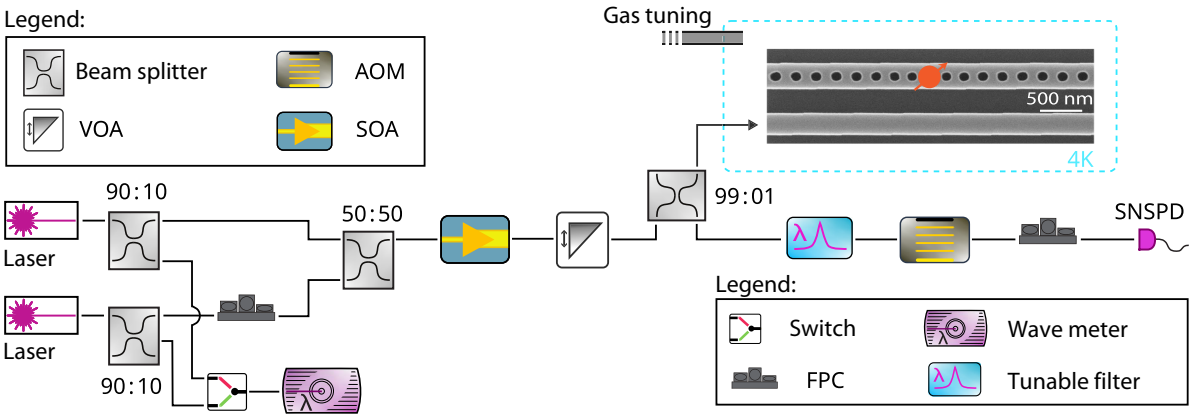


FIG. 5. The setup for the spectral hole burning. AOM, acousto-optic modulator; SOA, semiconductor optical amplifier; FPC, fiber polarization controller.

(BS), a semiconductor optical amplifier (SOA, Aerodiode SOA-3PI, 1-ns rise time) creates the optical pulses and a variable optical attenuator (VOA, Agiltron) controls the pulse power. After the fiber polarization controller (FPC), which is used to align the polarization to the optical waveguide, the laser pulses are routed to the device inside a 4-K cryostat (Montana S200) using a 99 : 01 BS. The coupling to the device is done with a lensed fiber (OZ Optics) mounted on nanopositioners (Attocube ANPx101/LT and ANPz102/LT). The light reflected from the device and emitted from the T-center is spectrally filtered using a tunable bandpass filter (WL photonics, flat top with bandwidth of 0.5 nm). The strong control light is time gated using an AOM (Aerodiode AOM model 10, rise time 10 ns). A final FPC aligns the polarization to maximize the T-center signal on the superconducting nanowire single-photon detector (SNSPD) (Quantum Opus, quantum efficiency 60%). Transistor-transistor logic control pulses are generated with Swabian Instruments Pulse Streamer 8/2, and SNSPD clicks are recorded with a Swabian Instruments Time Tagger Ultra.

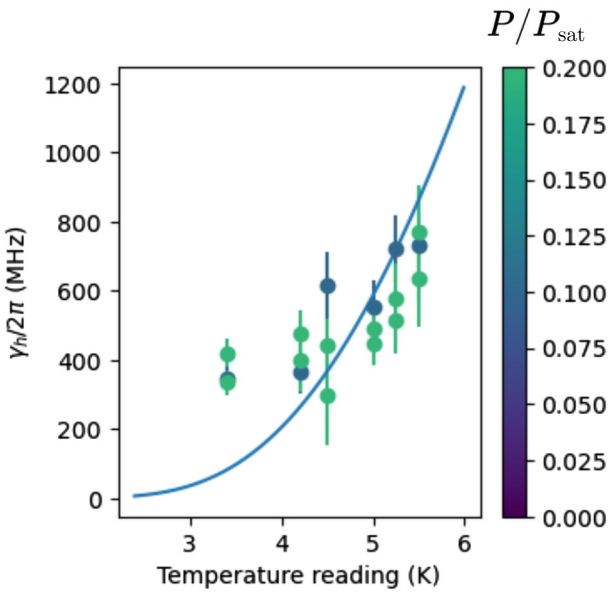


FIG. 6. The spectral hole-burning linewidth with the temperature of the cryostat. The spectral hole-burning linewidth for several temperatures of the cryostat: from a base temperature of 3.4 K to 5.5 K. The colors of the data points represent different powers relative to the saturation power P_{sat}. The blue curve is the expected thermal linewidth assuming TX_0-TX_1 splitting of 1.76 meV. All error bars are one standard deviation.

A steel hose (outer diameter 1/16 in.) is used to gas tune the cavity to the T-center resonance. Since it can only red shift the cavity, we use the laser on resonance with the cavity to blue shift it and maintain the resonance condition (for more details, see Ref. [21]).

We have measured the spectral hole burning for several chamber temperatures, using the same sequence as in Fig. 2. We report the results in Fig. 6 for several optical powers (relative to the saturation power). We note that the trend of the linewidth follows the expected trend (the solid blue line, from the thermal broadening [5]) quite closely for higher chamber temperatures (up to 5.5 K). For lower temperatures, we note a plateau around the hole width of 400 MHz, indicating a higher effective temperature of the device than the base temperature of the cryostat. This set of data is taken in a separate cooldown from Fig. 2(b), which may result in an increased device temperature and thus a larger hole width.

APPENDIX B: CHECK-PROBE SPECTROSCOPY: SETUP AND POWER DEPENDENCE

We use the setup depicted in Fig. 7 for the check-probe spectroscopy. The setup is similar to the one for the spectral hole burning. We describe only the differences here. Each laser is followed by its dedicated SOA (Aerodiode SOA-3PI, 1-ns rise time) and VOA (Agiltron MSOA)

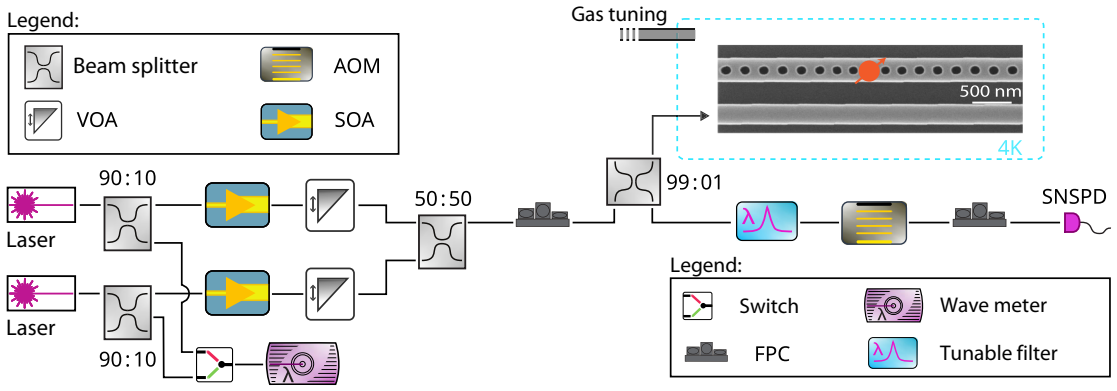


FIG. 7. The setup for the check-probe spectroscopy. VOA, variable optical attenuator; AOM, acousto-optic modulator; SOA, semiconductor optical amplifier; FPC, fiber polarization controller.

to independently create optical pulses and set the power (measured at the unused arm of the 50 : 50 BS with a power meter—Thorlabs S154C). Note that the high on-off ratio of the SOAs allows for a small background in the measurements reported in Fig. 3, enabling a negligible amount of spurious coincidences. After the combination at the 50 : 50 BS and the FPC, the setup is identical to the one described in Appendix A.

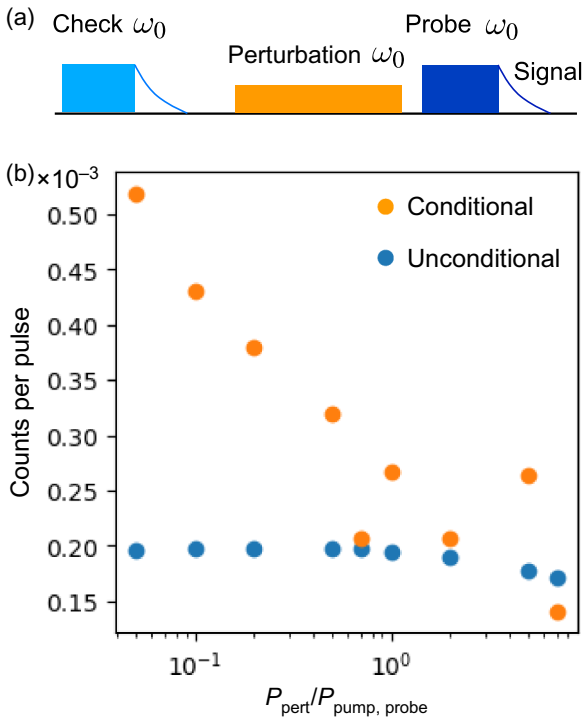


FIG. 8. The power dependence of laser-induced spectral diffusion. (a) The pulse sequence: a check-probe scheme is used, with a long perturbation pulse in between. (b) The conditional (orange) and unconditional (blue) counts per pulse as a function of the perturbation-laser power.

Similarly to Fig. 4, we use a check-probe scheme to assess the laser-induced spectral diffusion caused by a long laser pulse. In Fig. 8(a), the pulse sequence consists of a check and a probe pulse (locked at the center frequency ω_0, pulse length of 200 ns, shown in blue), and an 8-μs-long perturbation pulse in between the check and probe pulse (locked at ω_0, shown in orange). The single-photon arrival time is represented by the blue line with exponential decay labeled "signal." We use a fixed pump-probe power of 2.5% of the saturation power.

Since a full scan of the laser wavelength across the T-center PLE span would be too time-consuming, we use, as done for Fig. 3(e), the CPP at the center frequency to infer the linewidth. We report the results in Fig. 8(b). As in the main text, we calculate the conditional and unconditional CPP to compare the influence of the perturbation pulse. Since the conditional CPP decreases with increasing power of the perturbation pulse, we can infer an increase in the spectral diffusion.

The perturbation pulse mimics the initialization step of the T-center spin using optical pumping. We compare the laser power of the perturbation pulse to the power we expect for optical pumping of the spin [3]. Although the actual optical-pumping power needs to be calibrated for the specific setup, it is likely the optical pumping will lead to a considerable increase in spectral diffusion. Therefore, it could be challenging to herald with an initial pulse and maintain the resonance frequency through the spin initialization process via optical pumping. More careful calibration and pulse sequence design will be necessary in this case.

APPENDIX C: SPECTRAL DIFFUSION RATE

The spectral diffusion from charge-trap reconfiguration has been modeled using random-walk theory [19,30]. The model suggests that the inhomogeneous linewidth is determined by a Lorentzian propagator capturing the spectral diffusion and its homogeneous linewidth. The linewidth

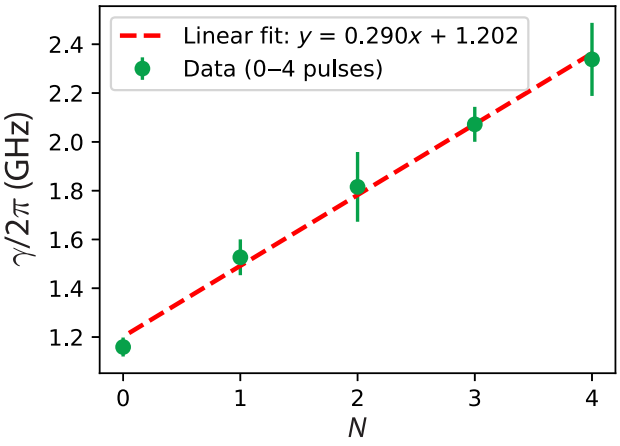


FIG. 9. Linear fitting of the conditional linewidth in Fig. 4(b) at laser pulse numbers varying from 0 to 4.

of the Lorentzian propagator grows linearly with time at the beginning, resulting in a linear growth of the spectral-diffusion-dominated inhomogeneous linewidth $\gamma = \gamma_d \tau$, where γ_d is the spectral diffusion rate.

By fitting the conditional linewidth under the first four perturbation pulses in Fig. 4(b), we obtain the spectral diffusion of 0.29 GHz per laser pulse (Fig. 9). Given 200 ns of laser pulse length, the spectral diffusion rate under 0.25 nW of waveguide power is $\gamma_d/2\pi = 1.45\,\mathrm{GHz}/\mu\mathrm{s}$.

[1] W. Redjem, A. Durand, T. Herzig, A. Benali, S. Pezzagna, J. Meijer, A. Y. Kuznetsov, H. S. Nguyen, S. Cueff, J. M. Gérard, I. Robert-Philip, B. Gil, D. Caliste, P. Pochet, M. Abbarchi, V. Jacques, A. Dréau, and G. Cassabois, Single artificial atoms in silicon emitting at telecom wavelengths, Nat. Electron. **3**, 738 (2020).

[2] A. Durand, Y. Baron, W. Redjem, T. Herzig, A. Benali, S. Pezzagna, J. Meijer, A. Y. Kuznetsov, J.-M. Gérard, I. Robert-Philip, M. Abbarchi, V. Jacques, G. Cassabois, and A. Dréau, Broad diversity of near-infrared single-photon emitters in silicon, Phys. Rev. Lett. **126**, 083602 (2021).

[3] D. B. Higginbottom *et al.*, Optical observation of single spins in silicon, Nature **607**, 266 (2022).

[4] PsiQuantum team, A manufacturable platform for photonic quantum computing, Nature **641**, 876 (2025).

[5] L. Bergeron, C. Chartrand, A. T. K. Kurkjian, K. J. Morse, H. Riemann, N. V. Abrosimov, P. Becker, H. J. Pohl, M. L. W. Thewalt, and S. Simmons, Silicon-integrated telecommunications photon-spin interface, PRX Quantum **1**, 020301 (2020).

[6] F. Afzal *et al.*, Distributed quantum computing in silicon, arXiv:2406.01704.

[7] H. K. Beukers, M. Pasini, H. Choi, D. Englund, R. Hanson, and J. Borregaard, Remote-entanglement protocols for stationary qubits with photonic interfaces, PRX Quantum **5**, 010202 (2024).

[8] K. Ngan and S. Sun, Performance analysis of different photon-mediated entanglement generation schemes under optical dephasing and spectral diffusion, Phys. Rev. A **112**, 012424 (2025).

[9] L. V. H. Rodgers, L. B. Hughes, M. Xie, P. C. Maurer, S. Kolkowitz, A. C. B. Jayich, and N. P. de Leon, Materials challenges for quantum technologies based on color centers in diamond, MRS Bull. **46**, 623 (2021).

[10] L. Orphal-Kobin, C. G. Torun, J. M. Bopp, G. Pieplow, and T. Schröder, Coherent microwave, optical, and mechanical quantum control of spin qubits in diamond, Adv. Quantum Technol. **8**, 2300432 (2025).

[11] J. Bader, H. Arianfard, A. Peruzzo, and S. Castelletto, Analysis, recent challenges and capabilities of spin-photon interfaces in silicon carbide-on-insulator, npj Nanophotonics **1**, 29 (2024).

[12] D. M. Lukin, M. A. Guidry, and J. Vučković, Integrated quantum photonics with silicon carbide: Challenges and prospects, PRX Quantum **1**, 020102 (2020).

[13] S. Castelletto and A. Boretti, Silicon carbide color centers for quantum applications, J. Phys.: Photonics **2**, 022001 (2020).

[14] J. Wolters, N. Sadzak, A. W. Schell, T. Schröder, and O. Benson, Measurement of the ultrafast spectral diffusion of the optical transition of nitrogen vacancy centers in nano-size diamond using correlation interferometry, Phys. Rev. Lett. **110**, 027401 (2013).

[15] A. Faraon, C. Santori, Z. Huang, V. M. Acosta, and R. G. Beausoleil, Coupling of nitrogen-vacancy centers to photonic crystal cavities in monocrystalline diamond, Phys. Rev. Lett. **109**, 033604 (2012).

[16] M. Ruf, M. IJspeert, S. Van Dam, N. De Jong, H. Van Den Berg, G. Evers, and R. Hanson, Optically coherent nitrogen-vacancy centers in micrometer-thin etched diamond membranes, Nano Lett. **19**, 3987 (2019).

[17] L. Orphal-Kobin, K. Unterguggenberger, T. Pregnolato, N. Kemf, M. Matalla, R.-S. Unger, I. Ostermay, G. Pieplow, and T. Schröder, Optically coherent nitrogen-vacancy defect centers in diamond nanostructures, Phys. Rev. X **13**, 011042 (2023).

[18] L. Robledo, H. Bernien, I. Van Weperen, and R. Hanson, Control and coherence of the optical transition of single nitrogen vacancy centers in diamond, Phys. Rev. Lett. **105**, 177403 (2010).

[19] G. L. Van De Stolpe, L. J. Feije, S. J. H. Loenen, A. Das, G. M. Timmer, T. W. De Jong, and T. H. Taminiau, Check-probe spectroscopy of lifetime-limited emitters in bulk-grown silicon carbide, npj Quantum Inf. **11**, 31 (2025).

[20] A. DeAbreu, C. Bowness, A. Alizadeh, C. Chartrand, N. A. Brunelle, E. R. MacQuarrie, N. R. Lee-Hone, M. Ruether, M. Kazemi, A. T. K. Kurkjian, S. Roorda, N. V. Abrosimov, H. J. Pohl, M. L. W. Thewalt, D. B. Higginbottom, and S. Simmons, Waveguide-integrated silicon T centres, Opt. Express **31**, 15045 (2023).

[21] L. Komza, X. Zhang, H. Song, Y.-L. Tang, X. Wei, and A. Sipahigil, Multiplexed color centers in a silicon photonic cavity array, Optica **12**, 1400 (2025).

[22] C.-M. Lee, F. Islam, S. Harper, M. A. Buyukkaya, D. Higginbottom, S. Simmons, and E. Waks, High-efficiency single photon emission from a silicon T-center in a nanobeam, ACS Photonics **10**, 3844 (2023).

[23] A. Johnston, U. Felix-Rendon, Y.-E. Wong, and S. Chen, Cavity-coupled telecom atomic source in silicon, Nat. Commun. **15**, 2350 (2024).
[24] G. Pieplow, C. G. Torun, C. Gurr, J. H. Munns, F. M. Herrmann, A. Thies, T. Pregnolato, and T. Schröder, Quantum electrometer for time-resolved material science at the atomic lattice scale, Nat. Commun. **16**, 6435 (2025).
[25] W. Ji, Z. Liu, Y. Guo, Z. Hu, J. Zhou, S. Dai, Y. Chen, P. Yu, M. Wang, K. Xia, F. Shi, Y. Wang, and J. Du, Correlated sensing with a solid-state quantum multisensor system for atomic-scale structural analysis, Nat. Photonics **18**, 230 (2024).
[26] D. R. Candido and M. E. Flatté, Suppression of the optical linewidth and spin decoherence of a quantum spin center in a p-n diode, PRX Quantum **2**, 040310 (2021).
[27] C. P. Anderson, A. Bourassa, K. C. Miao, G. Wolfowicz, P. J. Mintun, A. L. Crook, H. Abe, J. U. Hassan, N. T. Son, T. Ohshima, and D. D. Awschalom, Electrical and optical control of single spins integrated in scalable semiconductor devices, Science **366**, 1225 (2019).
[28] T. Delord, R. Monge, and C. A. Meriles, Correlated spectroscopy of electric noise with color center clusters, Nano Lett. **24**, 6474 (2024).
[29] F. Dolde, M. W. Doherty, J. Michl, I. Jakobi, B. Naydenov, S. Pezzagna, J. Meijer, P. Neumann, F. Jelezko, N. B. Manson, *et al.*, Nanoscale detection of a single fundamental charge in ambient conditions using the NV^- center in diamond, Phys. Rev. Lett. **112**, 097603 (2014).
[30] G. Zumofen and J. Klafter, Spectral random walk of a single molecule, Chem. Phys. Lett. **219**, 303 (1994).
[31] A. E. Siegman, *Lasers* (University Sciences Books, Mill Valley, CA, 1986).
[32] M. Pompili, S. L. N. Hermans, S. Baier, H. K. C. Beukers, P. C. Humphreys, R. N. Schouten, R. F. L. Vermeulen, M. J. Tiggelman, L. dos Santos Martins, B. Dirkse, S. Wehner, and R. Hanson, Realization of a multinode quantum network of remote solid-state qubits, Science **372**, 259 (2021).
[33] S. L. N. Hermans, M. Pompili, H. K. C. Beukers, S. Baier, J. Borregaard, and R. Hanson, Qubit teleportation between non-neighbouring nodes in a quantum network, Nature **605**, 663 (2022).
[34] H. Bernien, B. Hensen, W. Pfaff, G. Koolstra, M. S. Blok, L. Robledo, T. H. Taminiau, M. Markham, D. J. Twitchen, L. Childress, and R. Hanson, Heralded entanglement between solid-state qubits separated by three metres, Nature **497**, 86 (2013).
[35] J. M. Brevoord, L. D. Santis, T. Yamamoto, M. Pasini, N. Codreanu, T. Turan, H. K. Beukers, C. Waas, and R. Hanson, Heralded initialization of charge state and optical-transition frequency of diamond tin-vacancy centers, Phys. Rev. Appl. **21**, 054047 (2024).
[36] M. H. Abobeih, Y. Wang, J. Randall, S. J. H. Loenen, C. E. Bradley, M. Markham, D. J. Twitchen, B. M. Terhal, and T. H. Taminiau, Fault-tolerant operation of a logical qubit in a diamond quantum processor, Nature **606**, 884 (2022).
[37] L. Robledo, L. Childress, H. Bernien, B. Hensen, P. F. Alkemade, and R. Hanson, High-fidelity projective read-out of a solid-state spin quantum register, Nature **477**, 574 (2011).
[38] F. Islam, C.-M. Lee, S. Harper, M. H. Rahaman, Y. Zhao, N. K. Vij, and E. Waks, Cavity-enhanced emission from a silicon T center, Nano Lett. **24**, 319 (2024).
[39] A. Stirling, A. Pasquarello, J.-C. Charlier, and R. Car, Dangling bond defects at Si-SiO_2 interfaces: Atomic structure of the P_{b1} center, Phys. Rev. Lett. **85**, 2773 (2000).
[40] C. Boehme, F. Friedrich, and K. Lips, A pulsed EDMR study of charge trapping at Pb centers, MRS Online Proc. Lib. (OPL) **864**, E11 (2005).
[41] K. Kato, T. Yamasaki, and T. Uda, Origin of P_{b1} center at SiO_2/Si (100) interface: First-principles calculations, Phys. Rev. B: Condens. Matter Mater. Phys. **73**, 073302 (2006).
[42] K. Brower, Kinetics of H_2 passivation of P_b centers at the (111) Si-SiO_2 interface, Phys. Rev. B **38**, 9657 (1988).
[43] C. K. Hong, Z. Y. Ou, and L. Mandel, Measurement of subpicosecond time intervals between two photons by interference, Phys. Rev. Lett. **59**, 2044 (1987).
[44] C. Santori, D. Fattal, J. Vučković, G. S. Solomon, and Y. Yamamoto, Indistinguishable photons from a single-photon device, Nature **419**, 594 (2002).
[45] O. Gazzano, S. M. de Vasconcellos, C. Arnold, A. Nowak, E. Galopin, I. Sagnes, L. Lanco, A. Lemaître, and P. Senellart, Bright solid-state sources of indistinguishable single photons, Nat. Commun. **4**, 1425 (2013).
[46] L. Komza, P. Samutpraphoot, M. Odeh, Y.-L. Tang, M. Mathew, J. Chang, H. Song, M.-K. Kim, Y. Xiong, G. Hautier, and A. Sipahigil, Indistinguishable photons from an artificial atom in silicon photonics, Nat. Commun. **15**, 6920 (2024).
[47] C. Bowness, S. A. Meynell, M. Dobinson, C. Clear, K. Jooya, N. Brunelle, M. Keshavarz, K. Boos, M. Gascoine, S. Taherizadegan, *et al.*, Laser-induced spectral diffusion and excited-state mixing of silicon T centers, PRX Quantum **6**, 030350 (2025).
[48] X. Zhang, N. Fiaschi, L. Komza, H. Song, T. Schenkel, and A. Sipahigil, Data for "Laser-induced spectral diffusion of T centers in silicon nanophotonic devices" (2025), https://doi.org/doi:10.5281/zenodo.16844939.